In vivo evaluation of [F-18]FEAnGA-Me

Antunes, Inês F.; Haisma, Hidde J.; Elsinga, Philip H.; Sijbesma, Jurgen W. A.; van Waarde, Aren; Willemsen, Antoon T. M.; Dierckx, Rudi A.; de Vries, Erik F. J.

Published in:
Nuclear Medicine and Biology

DOI:
10.1016/j.nucmedbio.2012.02.002

Publication date:
2012

Nuclear Medicine and Biology 39 (2012) 854–863

Contents lists available at SciVerse ScienceDirect

Nuclear Medicine and Biology

journal homepage: www.elsevier.com/locate/nucmedbio

In vivo evaluation of [^{18}F]FEAnGA-Me: a PET tracer for imaging β-glucuronidase (β-GUS) activity in a tumor/inflammation rodent model

Inês F. Antunes[a,*], Hidde J. Haisma[b], Philip H. Elsinga[a], Jurgen W.A. Sijbesma[a], Aren van Waarde[a], Antoon T.M. Willemsen[a], Rudi A. Dierckx[a], Erik F.J. de Vries[a]

[a] Department of Nuclear Medicine and Molecular Imaging, University Medical Center Groningen, University of Groningen, 9700 RB Groningen, The Netherlands
[b] Department of Pharmaceutical Gene Modulation, University Center for Pharmacy, University of Groningen, A. Deusinglaan 1, 9713 AV Groningen, The Netherlands

ARTICLE INFO

Article history:
Received 11 July 2011
Received in revised form 2 January 2012
Accepted 11 February 2012

Keywords:
Prodrug
β-glucuronidase
Pharmacokinetics
PET
Necrosis and inflammation

ABSTRACT

Introduction: The PET tracer, 1-*O*-(4-(2-fluoroethyl-carbamoyloxymethyl)-2-nitrophenyl)-*O*-β-D-glucopyronuronate ([^{18}F]FEAnGA), was recently developed for PET imaging of extracellular β-glucuronidase (β-GUS). However, [^{18}F]FEAnGA exhibited rapid renal clearance, which resulted in a relatively low tracer uptake in the tumor. To improve the pharmacokinetics of [^{18}F]FEAnGA, we developed its more lipophilic methyl ester analog, [^{18}F]FEAnGA-Me.
Methods: [^{18}F]FEAnGA-Me was obtained by alkylation of the *O*-protected glucuronide methyl ester precursor with [^{18}F]-fluoroethylamine ([^{18}F]FEA), followed by removal of the acetate protecting groups with NaOMe/MeOH. The PET tracer was evaluated by in vitro and in vivo studies.
Results: [^{18}F]FEAnGA-Me was obtained in 5%–10% overall radiochemical yield. It is 10-fold less hydrophilic than [^{18}F]FEAnGA and it is stable in PBS and in the presence of β-GUS for 1 h. However, in the presence of esterase or plasma [^{18}F]FEAnGA-Me is converted to [^{18}F]FEAnGA, and subsequently converted to [^{18}F]FEA by β-GUS. MicroPET studies in Wistar rats bearing a C6 glioma and a sterile inflammation showed similar uptake in tumors after injection of either [^{18}F]FEAnGA-Me or [^{18}F]FEAnGA. Both tracers had a rapid two-phase clearance of total plasma radioactivity with a half-life of 1 and 8 min. The [^{18}F]FEAnGA fraction generated from [^{18}F]FEAnGA-Me by in vivo hydrolysis had a circulation half-life of 1 and 11 min in plasma. Similar distribution volume in the viable part of the tumor was found after injection of either [^{18}F]FEAnGA-Me or [^{18}F]FEAnGA.
Conclusion: The imaging properties of [^{18}F]FEAnGA-Me were not significantly better than those of [^{18}F]FEAnGA. Therefore, other strategies should be applied in order to improve the kinetics of these tracers.

1. Introduction

Glucuronide-drug conjugates exhibit lower toxicity towards normal cells than the corresponding native drugs. However, glucuronide-drug conjugates are susceptible to enzymatic cleavage by β-GUS, resulting in the in situ generation of highly cytotoxic drugs. Since tumors and inflammatory lesions have increased levels of β-GUS, glucuronide conjugates have been investigated as tools to deliver drugs to the target site.

For a better understanding of the mechanisms of action and metabolic conversion of these prodrugs, we have recently synthesized a radiopharmaceutical, 1-*O*-(4-(2-fluoroethyl-carbamoyloxymethyl)-2-nitrophenyl)-*O*-β-D-glucopyronuronate ([^{18}F]FEAnGA), for non-invasive PET imaging of extracellular β-GUS activity [1]. Micro-PET with [^{18}F]FEAnGA could clearly visualize enhanced β-GUS levels, in particular in large tumors with necrotic areas, whereas uptake in other organs was very low (except kidneys and bladder). The distribution volume (DV_T) of [^{18}F]FEAnGA in tumors correlated well with the conversion of [^{18}F]FEAnGA by the β-GUS enzyme. However, because of the highly hydrophilic character of [^{18}F]FEAnGA (logD = −1.61), the PET tracer is very rapidly excreted via the kidneys into the urine. This rapid renal clearance resulted in a relatively low absolute tracer uptake in the tumor [2].

The disadvantage of rapid renal clearance was also found for prodrugs such as DOX-GA3 and DNR-GA3 [3,4]. To reduce renal clearance, de Graaf et al. converted DOX-GA3 to its methyl ester (DOX-mGA3), which is substantially less hydrophilic [5]. The glucuronide conjugate is negatively charged at physiological pH, whereas the corresponding methyl ester is a neutral molecule. Slow release of DOX-GA3 through conversion of its methyl ester by esterase activity in blood resulted in a prolonged circulation half-life of DOX-GA3. Intravenous administration of DOX-mGA3 in tumor bearing mice resulted in a 2.7-fold increase in the delivery (area under the concentration versus time curve (AUC) from 0.5 to 2 h) of doxorubicin to the tumor, as compared to administration of DOX-GA3. Therefore,

* Corresponding author. Department of Nuclear Medicine and Molecular Imaging, University Medical Center Groningen, University of Groningen, 9700 RB Groningen, The Netherlands. Tel.: +31 50 3619309; fax: +31 50 3611687.
E-mail addresses: i.farinha.antunes@umcg.nl, i_antunes@yahoo.com (I.F. Antunes).

0969-8051/$ – see front matter © 2012 Elsevier Inc. All rights reserved.
doi:10.1016/j.nucmedbio.2012.02.002

we hypothesized that a similar approach could increase the delivery of [^{18}F]FEAnGA as well. Therefore, we now synthesized its less hydrophilic methyl ester of [^{18}F]FEAnGA, called [^{18}F]FEAnGA-Me. When administered in vivo, the methyl group of [^{18}F]FEAnGA-Me should be removed by carboxylesterase activity in plasma to give the original PET tracer [^{18}F]FEAnGA, which could in turn be activated by β-GUS at the target site (Scheme 1) and release 2-[^{18}F]fluoroethylamine ([^{18}F]FEA). The slow release of [^{18}F]FEAnGA after administration of [^{18}F]FEAnGA-Me might result in improved pharmacokinetics of the PET tracer in vivo, resulting in a higher absolute tracer uptake in tumors.

In the present study, we describe the labeling of [^{18}F]FEAnGA-Me and its stability in vitro. In addition, we analyzed the in vitro conversion of [^{18}F]FEAnGA-Me to [^{18}F]FEAnGA by esterase activity and determined whether [^{18}F]FEAnGA-Me could be converted to [^{18}F]FEAnGA and [^{18}F]FEA in vivo. Finally, the PET imaging characteristics of [^{18}F]FEAnGA-Me were compared with the original PET tracer [^{18}F]FEAnGA.

2. Materials and methods

Reagents and solvents were obtained from commercial suppliers (Sigma-Aldrich and Fluka, Zwijndrecht, the Netherlands and Merck, Darmstadt, Germany) and used without further purification. The reference compounds, FEAnGA-Me and FEAnGA were prepared as previously described [1]. For radiolabeled compounds, the detection on the TLC was performed with Cyclone phosphor storage screens (multisensitive, Packard, PerkinElmer Life and Analytica Science). These screens were exposed to the TLC strips (60 s for in vitro experiments and 20 min for in vivo experiments), subsequently read out using a Cyclone phosphor storage imager (PerkinElmer) and analyzed with OptiQuant software. HPLC purifications were performed with an Elite LaChrom VWR Hitachi L-2130 pump system using a Phenomenex Prodigy C18-column, connected to a UV-spectrometer (Elite LaChrom VWR Hitachi L-2400 UV detector) set at 254 nm and a Bicron frisk-tech radiation detector. Radioactivity measurements for logD determination and cell studies were done using an automated gamma counter (Compugamma, LKB Wallac). Absorbance measurements in the enzyme assays were performed with a UV-spectrophotometer (Waters 2487 dual wavelength absorbance detector).

2.1. Radiosynthesis of [^{18}F]FEAnGA-Me (Scheme 2)

Aqueous [^{18}F]fluoride was produced via the ^{18}O (p,n)^{18}F nuclear reaction by irradiation of [^{18}O]water with a Scanditronix MC-17 cyclotron. The [^{18}F]fluoride solution was passed through an activated SepPak Light Accell plus QMA anion exchange cartridge (Waters) to recover the [^{18}O]water. The [^{18}F]fluoride was eluted from the cartridge with 1 mL of K_2CO_3 (5 mg/mL) and collected in a vial with 20 mg Kryptofix[2.2.2.]. To this solution, 1 mL acetonitrile was added and the solvents were evaporated at 130 °C. The [^{18}F]KF/Kryptofix complex was dried 3 times by the addition of 0.5 mL acetonitrile, followed by evaporation of the solvent.

[^{18}F]FEA was prepared by fluorination of *N*-[2-(toluene-4-sulfonyloxy)-ethyl]-phtalimide (30 mg, 0.09 mmol) in 500 μL of acetonitrile at 110 °C, followed by deprotection with hydrazine hydrate (50 μl, 1.03 mmol) as described in the literature [6]. The resulting amine was distilled at 75 °C into an ice-cold solution of **1** (5 mg, 0.009 mmol) in acetonitrile (0.2 mL). The mixture was allowed to react at room temperature for 30 min. The product was dried at 40 °C for 2 min under a gentle argon flow. Deprotection of the hydroxyl groups was done by addition of 30 μL 0.5 M NAOMe/MeOH and incubation for 7 min at room temperature. The product was neutralized by the addition of 20 μL 1 M AcOH, diluted with 2 mL of distilled water and purified by HPLC using a semi-preparative Prodigy C_{18} reverse-phase column (5 μ, 10×250 mm; Phenomenex) with 17% ethanol in 0.025 M sodium phosphate buffer as the eluent (flow rate, 4 mL/min; retention time: [^{18}F]FEAnGA-Me = 21 min; [^{18}F]FEAnGA = 6.4 min and [^{18}F]FEA = 4.2 min). The radiolabeled compound [^{18}F]FEAnGA-Me was obtained in 5%–10% radiochemical yield from [^{18}F]fluoride (decay corrected) in 120 min. Quality control was performed by HPLC with a Symmetry C_{18} column [5 μm, 4.6×150 mm] with 15% acetonitrile in sodium phosphate buffer 2.5 mM as the eluent (flow rate, 1 mL/min; retention time: [^{18}F]FEAnGA-Me = 14 min). The specific activity of [^{18}F]FEAnGA-Me was 185 ± 71 GBq/μmol and the radiochemical purity was always >95%. [^{18}F]FEAnGA was prepared according to the literature [2] with a specific activity of 149 ± 33 GBq/μmol and the radiochemical purity was always >95%.

2.2. Stability of [^{18}F]EAnGA-Me

A sample of radiolabeled [^{18}F]FEAnGA-Me was dissolved in PBS (1 mL) and incubated at 37 °C. For 1 h, the stability of the radiolabeled [^{18}F]FEAnGA-Me was monitored by radio-TLC (R_f FEA = 0.1, R_f FEAnGA = 0.4 and R_f FEAnGA-Me = 1) (eluent: MeCN/H_2O 7:3). After elution, the TLC strips were analyzed by phosphor storage imaging. The screens were scanned with Cyclone phosphor storage system (PerkinElmer) and the percentage of intact [^{18}F]FEAnGA-Me as a function of the incubation period was calculated by ROI analysis using OptiQuant software. The experiment was performed in duplicate.

2.3. Distribution coefficient (Log $D_{7.4}$)

To determine the Log $D_{7.4}$ of [^{18}F]FEAnGA-Me an aliquot of 100 μL of HPLC purified [^{18}F]FEAnGA-Me solution was added to a mixture of *n*-octanol/PBS (4 mL:4 mL) at pH 7.4. The tubes were vortexed at room temperature for 30 s, followed by 30 min shaking in a water bath at 37 °C. Aliquots of 1 mL were drawn from both the *n*-octanol and aqueous phase. Radioactivity in both samples was counted using an automated gamma counter. The experiments were performed in triplicate.

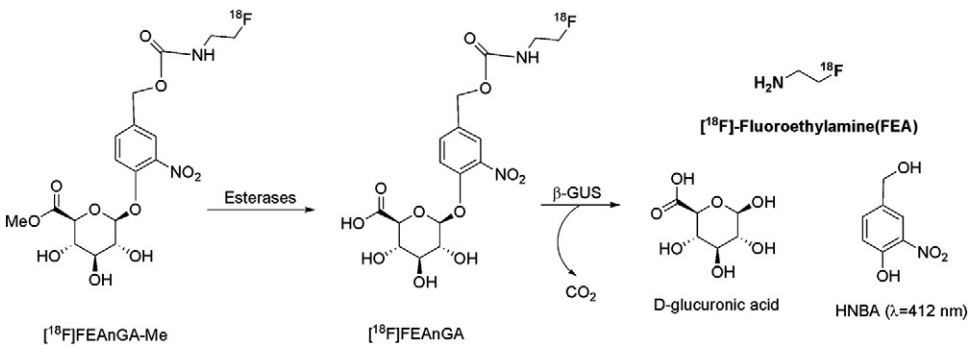

Scheme 1. General mechanism of activation of the prodrug tracer.

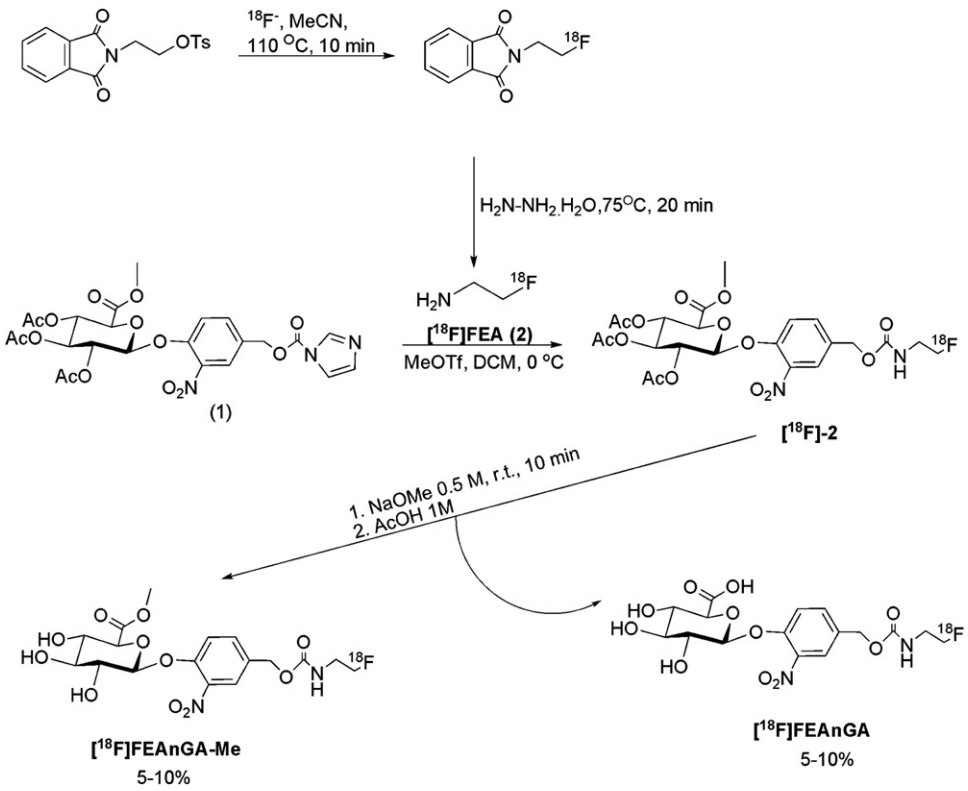

Scheme 2. Radiosynthesis of compound [^{18}F]FEAnGA-Me.

2.4. In vitro hydrolysis of FEAnGA-Me

To a solution of 0.1% bovine serum albumin (BSA), 200 μL (15U) of carboxylesterase of porcine liver (Sigma-Aldrich) and/or 10 μL (74U) *Escherichia coli* β-GUS (*E. coli* β-GUS) in 950 μL PBS (pH = 7), 50 μL of a 0.004 M solution of FEAnGA-Me was added (total volume 1 mL). The solutions were incubated in a water bath at 37 °C and 100 μL samples were collected at different time points between 1 min and 60 min after the start of incubation. The enzymatic activity was stopped by dilution of the samples in 300 μL of acetonitrile and cooling of the samples in ice. The release of 4-hydroxy-3-nitrobenzyl alcohol (HNBA) ($\varepsilon = 3460\ M^{-1}\ cm^{-1}$) was monitored by measuring the UV absorbance at 412 nm. The experiment was performed in duplicate.

2.5. In vitro hydrolysis of [^{18}F]FEAnGA-Me by plasma

To a 0.4 mL solution of PBS (pH = 7.4), or rat plasma with or without 10 μL (74U) *Escherichia coli* β-GUS, 0.1 mL of HPLC purified [^{18}F]FEAnGA-Me (2 ± 0.2 MBq; 11 ± 1 pmol) was added. The solutions were incubated in a water bath at 37 °C and 2 μL samples were collected at different time points between 30 s and 60 min after the start of incubation. The degradation of the radiolabeled [^{18}F]FEAnGA-Me was followed by radio-TLC (eluent: MeCN/H_2O 7:3). After elution, the TLCs were analyzed by phosphor storage imaging as described above. The experiment was performed in duplicate.

2.6. Cellular uptake of [^{18}F]FEAnGA-Me

C6 glioma cells were maintained in 5 mL Dulbecco's Modified Eagle Medium (DMEM) supplemented with 7.5% fetal bovine serum (FBS) in 25 cm^3 culture flasks. Cells were grown in a humidified atmosphere containing 5% CO_2 and were passaged every 3–4 days. For uptake experiments, cells were plated in triplicate in a 12-well plate at a density of 7×10^5 cells per well. After 24 h, the medium was discarded and 1 mL of PBS-GMC buffer (5.6 mM D-glucose, 0.49 mM $MgCl_2$ and 0.68 mM $CaCl_2$ in 100 mL phosphate-buffered saline (PBS)) per well was added, followed by the addition of 200 μL [^{18}F]FEAnGA-Me (ca. 250 kBq; ca. 1 pmol). In each series of 3 wells, either β-GUS (740 U), esterase (15 U) or a combination of β-GUS (740 U) and esterase (15 U) was added. After 60 min of incubation at 37 °C, the medium was collected, the cells washed with cold PBS (3 × 1 mL/well), harvested with trypsin (250 μL) and resuspended in 1750 μL of DMEM (total volume 2 mL/well). The cell suspensions and the medium were collected separately for each well and the radioactivity was measured using a gamma counter. For each well, the medium was analyzed for conversion of [^{18}F]FEAnGA-Me to [^{18}F]FEA by radio-TLC as described above.

2.7. Animal model

Wistar rats (6–8 weeks old) were obtained from Harlan (Lelystad, the Netherlands). The animals were provided with standard laboratory chow and tap water ad libitum. All studies were carried out in compliance with the local ethical guidelines for animal experiments. The protocols were approved by the Animal Ethics Committee of University of Groningen. The tumor-inflammation model was described previously [7,8]. Briefly, C6 glioma cells [2–3 × 10^6 cells in a 1:1 mixture of Matrigel and Dulbecco's minimal essential medium containing 7.5% fetal bovine serum] were subcutaneously injected into the right shoulder of male Wistar rats. At day 12, 0.1 mL of turpentine was intramuscularly injected into the thigh of the left hind leg of the same animal.

2.8. PET imaging and ex vivo biodistribution studies

In the tumor-inflammation model ($n = 14$), PET scans were performed on day 13 after inoculation. The rats were anesthetized with 2% isoflurane (5% induction, 2% maintenance; Pharmachemie BV, the Netherlands) and positioned in the small animal PET camera (Siemens, Focus 220) with the tumor in the field of view. Owing to

the small field-of-view of our microPET camera, it was not possible to obtain a whole body scan of the rat. Although the camera is equipped with a continuous bed motion option, this method is not suitable to obtain quantitative information, because attenuation correction is not feasible in this mode and the bed motion is relatively slow with respect to tracer kinetics, especially at the early time points. Moreover, imaging of the inflammatory lesions in the leg is difficult due to artifacts created by the high uptake in bladder, which would also be in the field-of-view. For the above mentioned reasons the PET scan was only performed in the tumor region. A transmission scan of 515 s with a Co-57 point source was obtained for the correction of attenuation and scatter by tissue. After the transmission scan was completed, [^{18}F]FEAnGA-Me (8.6 ± 0.7 MBq; 46 ± 4 pmol) or [^{18}F]FEAnGA (12.5 ± 2.2 MBq; 84 ± 5 pmol) was injected via the penile vein. Simultaneously with the injection of the PET tracer, an emission scan of 60 min was started. After completion of the emission scan, the rats were sacrificed by extirpation of the heart, while still being under deep isoflurane anesthesia. Several tissues, peripheral organs, tumor and inflamed muscle were excised and blood was collected. Plasma and red blood cells were obtained from the blood sample by centrifugation (20 min at 6000 *g*). All tissue samples and plasma were weighed and the amount of radioactivity was determined with a gamma counter (LKB Wallac, Turku, Finland). Tracer uptake is expressed as standardized uptake value (SUV), which is defined as: [tissue activity concentration (MBq/g) × body weight (g) / injected dose (MBq)]. It was assumed that 1 cm^3 of tissue equals 1 g.

2.9. Pharmacokinetics studies

Wistar rats (n = 22) bearing a C6 tumor were anesthetized with isoflurane (5% induction, 2% maintenance) and a canula was inserted into the femoral artery for collection of blood samples. Animals were placed in the PET camera with the tumor in the center of the field of view. Simultaneously with the injection of either [^{18}F]FEAnGA-Me (7.0 ± 0.9 MBq; 38 ± 5 pmol) or [^{18}F]FEAnGA (7.4 ± 0.5 MBq; 50 ± 3 pmol), a dynamic PET scan was started as described above. During the 60 min PET scan, blood samples of 100 μL were taken at 15, 30, 45, 60, 75, 90, 120, 150, 300, 450, 600, 1800, 3600 s after tracer injection. After a blood sample was taken, 100 μL of heparinized saline was injected via the artery canula to prevent large changes in blood pressure. The blood samples were centrifuged at 6000 rpm for 10 min and 50 μL of plasma was collected. The activity in plasma was measured with a gamma counter (LKB Wallac, Turku, Finland). The plasma–activity curves were corrected for decay. The rats were sacrificed after the scans and the tumors were excised and weighed. The radioactivity in the tumors was measured with a gamma counter and converted to SUV.

2.10. PET image analysis

The list mode data of the emission scans were separated into 17 frames. Emission sinograms were iteratively reconstructed (OSEM2D, 4 iterations, 16 subsets) after being normalized, corrected for attenuation, and corrected for radioactive decay. Three-dimensional regions of interest (3D-ROIs) were generated automatically using the intensity threshold method from Inveon Research Workplace software package (Inveon, Siemens, USA) [9,10]. Briefly, the last 9 frames (10–60 min) were summed and an ROI of the viable part of the tumor was generated automatically with a 50% threshold using a region growing method, i.e. only pixels with tracer uptake greater than 50% of the maximum value within the lesion were included. The resulting ROIs were used on the original data set to create the corresponding 0–60 min time–activity curves (TACs). A second ROI was drawn around the whole tumor to obtain the total tumor volume (V_t; cm^3), using standard software (Inveon, Siemens, USA). In those animals where plasma input curves were obtained through arterial sampling, pharmacokinetic modeling of the tissue TACs was performed using standard software (Inveon, Siemens, USA). The graphical Logan model was used to determine the distribution volume, DV_T, and a 2 tissue-compartment model fit was used to calculate the rate constants K_1-k_4 using a free blood volume.

2.11. Metabolite analysis

2.5 μL of each plasma sample was collected, applied on a TLC plate (Merck F-254 silica gel) and eluted with acetonitrile/water (7:3). After elution, TLC plates were analyzed by phosphor storage imaging. Exposed screens were scanned with a Cyclone phosphor storage system (PerkinElmer Life and Analytica Science) and the percentage of conversion of [^{18}F]FEAnGA-Me as a function of time was calculated by ROI analysis using OptiQuant software.

2.12. Conversion of [^{18}F]FEAnGA-Me to [^{18}F]FEA with the release of HNBA (Scheme 1)

Part of the tumors (containing both the rim and the necrotic core, 0.12 ± 0.04 g) excised from the sampled animals was homogenized in 2 mL of phosphate buffered saline (PBS). The homogenates were centrifuged (10 min, 3000 rpm, 4 °C) and the supernatant was collected and kept on ice. To the supernatant, 2 mL of cold acetonitrile was added to precipitate the remaining proteins. The samples were vortexed for 30 s and centrifuged at 3000 rpm for 10 min at 4 °C. A volume of 1.5 mL of the supernatant was added to 1.5 mL of cold NaOH 0.25 M and UV absorption was measured (Waters 2487 dual wavelength absorbance detector, 412 nm, aufs = 0.01). Absorption was converted in the concentration of HNBA, using a calibration curve. The absorption was corrected for the weight (mg) of the tumor sample. The measurements were performed in duplicate.

2.13. Statistical analysis

Statistical analyses were performed using Microsoft Excel 2003 and SigmaPlot (version 10.0; SPSS, Inc.). Differences in tumor accumulation between tracers were analyzed using the two-sided unpaired Student's t test. Differences in tracer accumulation between inflamed and healthy muscle were studied in the same animal to reduce variability between animals and therefore were analyzed using the two-sided paired Student's t test. Significance was reached when the P value was <.05. Correlations were calculated with the linear regression algorithm in SigmaPlot and were considered statistically significant whenever R^2>0.5 and P<.05. Throughout the manuscript values are presented as mean ± SEM.

3. Results

3.1. Labeling of [^{18}F]FEAnGA-Me

[^{18}F]FEAnGA-Me was prepared in analogy to [^{18}F]FEAnGA, by the reaction of [^{18}F]FEA **2** with the imidazolyl intermediate **1**, followed by removal of the acetate protecting groups with NaOMe/MeOH in anhydrous conditions. [^{18}F]FEAnGA-Me was obtained in a 10% ± 5% overall radiochemical yield (corrected for decay, based on [^{18}F] fluoride) with a total synthesis time of 120 min (Scheme 2). In addition, approximately equal amounts of fully hydrolyzed [^{18}F] FEAnGA were formed.

3.2. Properties of [^{18}F]FEAnGA-Me

The stability of [^{18}F]FEAnGA-Me in PBS, was evaluated at 37 °C. After 1 h of incubation, radio-TLC analysis showed that 95% of the tracer was still intact while 5% was hydrolyzed to [^{18}F]FEAnGA. We

then determined the lipophilicity of [^{18}F]FEAnGA-Me by measuring its *n*-octanol/water distribution coefficient (LogD) at pH 7.4. The logD of [^{18}F]FEAnGA-Me was found to be -0.58 ± 0.0002.

3.3. In vitro hydrolysis of FEAnGA-Me/[^{18}F]FEAnGA-Me

The enzymatic processing of FEAnGA-Me was first studied using commercially available bacterial *Escherichia coli* β-GUS and porcine liver carboxylesterase. Fig. 1 indicates that incubation of FEAnGA-Me with the combination of esterase and *E. coli* β-GUS resulted in 80% conversion to FEA and 4-hydroxy-3-nitrobenzyl alcohol (HNBA), while in the presence of *E. coli* β-GUS alone, only 6% of FEAnGA-Me was converted to FEA and HNBA. This 6% conversion of FEAnGA-Me to FEAnGA in the absence of esterase was probably due to some spontaneous hydrolysis of the ester to the carboxylic acid. The liberation of 4-hydroxy-3-nitrobenzyl alcohol (HNBA) was measured by UV-spectrophotometry at 412 nm.

However, monitoring of the conversion of FEAnGA-Me to FEAnGA was not possible, since neither glucuronide shows UV absorption at this wavelength. Furthermore, we aimed to demonstrate that esterases in plasma are able to hydrolyze the glucuronide ester to the carboxylic acid. Therefore, we continued the hydrolysis analysis with the radioactive compound, [^{18}F]FEAnGA-Me. Radiolabeled [^{18}F]FEAnGA-Me was incubated in rat plasma. After 30 min, 99% of [^{18}F]FEAnGA-Me was converted to [^{18}F]FEAnGA, while no [^{18}F]FEAnGA was generated in 0.1% BSA in PBS. When [^{18}F]FEAnGA-Me was incubated in rat plasma supplemented with *E. coli* β-GUS, 50% cleavage of the tracer to [^{18}F]FEA was observed within 30 min (Fig. 2).

3.4. Cellular uptake of [^{18}F]FEAnGA-Me in C6 glioma cells

As depicted in Fig. 3, the cell-associated radioactivity was significantly increased by 60%, when C6 cells were incubated with [^{18}F]FEAnGA-Me in the presence of both *E. coli* β-GUS and esterase. After incubation of C6 cells with [^{18}F]FEAnGA-Me, cell-associated activity was not affected by either *E. coli* β-GUS or esterase alone. Furthermore, the radio-TLC analysis of the medium showed that in the presence of both *E. coli* β-GUS and esterase the conversion of [^{18}F]FEAnGA-Me to [^{18}F]FEA was 99%, while in the presence of *E. coli* β-GUS alone there was only 7% of conversion to [^{18}F]FEA. These results suggest that the increase in cell associated radioactivity is related with the conversion of [^{18}F]FEAnGA-Me to [^{18}F]FEA. The latter compound is thought to have a higher tendency to associate to the cells [1,2].

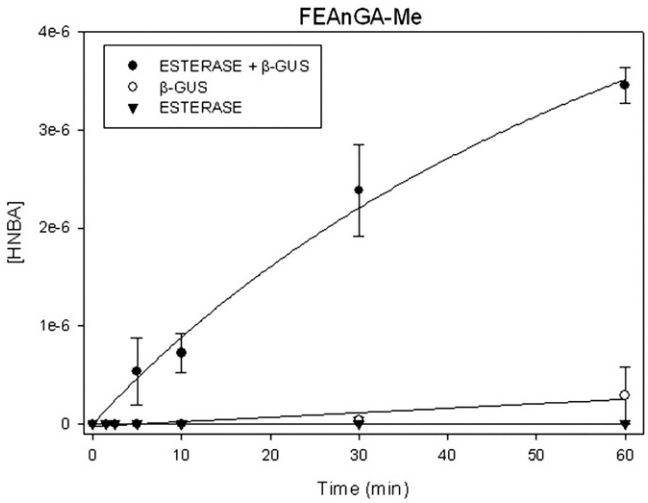

Fig. 1. In vitro release of the spacer HNBA from FEAnGA-Me and its quantification by UV absorption due to its yellow color (412 nm). FEAnGA-Me was exposed to either esterase or *E. coli* β-GUS alone, or a combination of both enzymes.

3.5. In vivo hydrolysis of [^{18}F]FEAnGA-Me

The hydrolysis of [^{18}F]FEAnGA-Me to [^{18}F]FEAnGA by plasma was also studied in tumor bearing rats. After injection into the rat, the fraction of [^{18}F]FEAnGA-Me present in plasma decreased rapidly to 50% in the first 2 min, followed by a plateau phase. After 10 min, [^{18}F]FEAnGA-Me was more slowly converted to [^{18}F]FEAnGA, with still 26% of the radioactivity in plasma being [^{18}F]FEAnGA-Me at the end of the study (60 min) (Fig. 4A). The fractions of radioactivity in plasma consisting of [^{18}F]FEAnGA and [^{18}F]FEA reached their maximum 60 min post injection (64% and 10%, respectively). When [^{18}F]FEAnGA was injected (Fig. 4B) only 12% was metabolized to [^{18}F]FEA, which is comparable to the amount of this compound found after injection of the methyl ester.

The plasma activity curves of [^{18}F]FEAnGA-Me, [^{18}F]FEAnGA and the [^{18}F]FEAnGA fraction generated by in vivo hydrolysis of [^{18}F]FEAnGA-Me are shown in Fig. 5. Exponential curve-fitting analysis of [^{18}F]FEAnGA-Me clearance showed a two-phase clearance with 25% of the injected activity having a half-life $(t_{1/2})_1$ of 1 ± 0.1 min and 75% of the injected activity having a half-life $(t_{1/2})_2$ of 8 ± 1 min ($n = 8$), which are similar to the plasma clearance of [^{18}F]FEAnGA (27% $(t_{1/2})_1 = 1 \pm 0.1$ min and 73% $(t_{1/2})_2 = 8 \pm 0.8$ min, $n = 14$). In addition, the [^{18}F]FEAnGA fraction generated in vivo by hydrolysis of [^{18}F]FEAnGA-Me (18% with $(t_{1/2})_1 = 1 \pm 0.2$ min and 82% with $(t_{1/2})_2 = 11 \pm 2$ min ($n = 8$)) had similar plasma clearance as [^{18}F]FEAnGA itself.

The AUC (1–60 min) of [^{18}F]FEAnGA-Me (3.5 ± 0.4) in plasma is similar to the AUC of [^{18}F]FEAnGA (3.3 ± 0.3), whereas the AUC of the [^{18}F]FEAnGA fraction generated in vivo by hydrolysis of [^{18}F]FEAnGA-Me (2.3 ± 0.5) was lower than the AUC of [^{18}F]FEAnGA (3.3 ± 0.3) itself, although this difference was not statistically significant.

3.6. PET study and ex vivo biodistribution

To test the potential of [^{18}F]FEAnGA-Me as a PET tracer for detecting β-GUS activity in vivo, a PET study was performed in rats bearing a C6 glioma and sterile inflammation. A microPET scan was performed in these rats after injection of either [^{18}F]FEAnGA-Me ($n = 6$) or [^{18}F]FEAnGA ($n = 8$), in order to compare both tracers. In the PET images (summed from 10 to 60 min, Fig. 6), [^{18}F]FEAnGA-Me showed a higher background activity when compared to [^{18}F]FEAnGA.

However, the time activity curves of [^{18}F]FEAnGA-Me and [^{18}F]FEAnGA in tumors were similar (Fig. 6). The accumulation of radioactivity in the viable part of the tumors after [^{18}F]FEAnGA-Me injection reached a maximum at 1.5 min post injection and afterwards decreased exponentially with a half-life of 16 ± 2 min, while after [^{18}F]FEAnGA injection, the accumulation of radioactivity in the viable part of the tumors decreased with a half-life of 24 ± 9 min (Fig. 6). In addition, the area under the curve (AUC) of [^{18}F]FEAnGA-Me in tumors (23 ± 6) was similar to the AUC of [^{18}F]FEAnGA in tumors (20 ± 4, $P = .65$).

To compare the distribution after [^{18}F]FEAnGA-Me or [^{18}F]FEAnGA injection, ex vivo biodistribution studies of both tracers were performed after the PET scan, i.e. at 60 min post injection. After injection of [^{18}F]FEAnGA-Me the uptake (SUV) in most of the peripheral organs was similar to the uptake in these organs after injection of [^{18}F]FEAnGA. However, uptake in the liver and kidneys was 3 times higher after injection of [^{18}F]FEAnGA-Me than after injection of [^{18}F]FEAnGA ($P < .05$) (Table 1). In the excised C6 tumors (2.35 ± 0.42 g), the uptake (SUV) was 0.13 ± 0.02 at 1 h after injection of [^{18}F]FEAnGA-Me, while tracer uptake was 0.13 ± 0.05 and

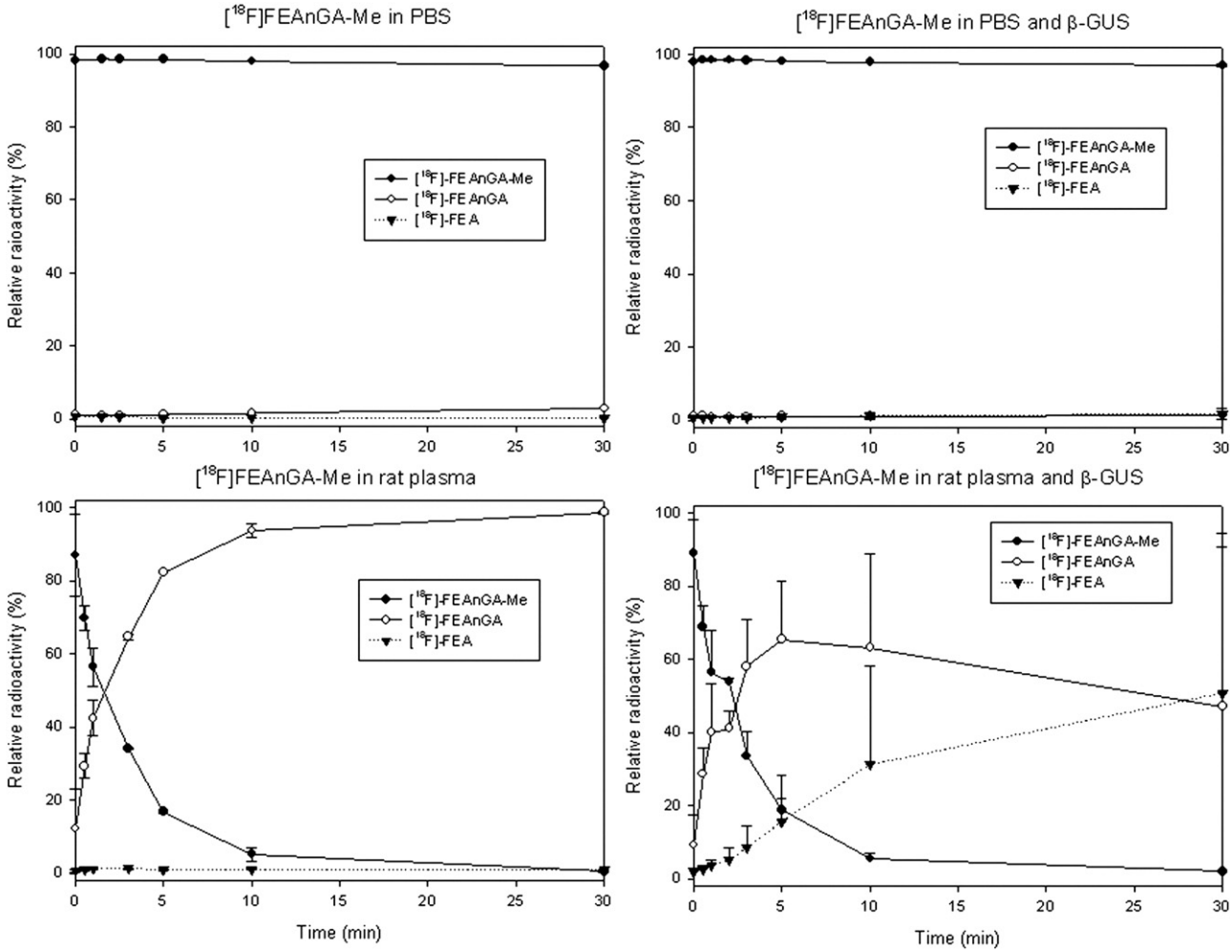

Fig. 2. Conversion of [^{18}F]FEAnGA-Me in: PBS (top left side), PBS with *E. coli* β-GUS (top right side), rat plasma (bottom left side) and rat plasma with *E. coli* β-GUS (bottom right side).

0.08 ± 0.02 in inflamed and healthy muscle, respectively. When injected with [^{18}F]FEAnGA the uptake was 0.13 ± 0.03 in the excised tumors (2.35 ± 0.65 g) and 0.07 ± 0.02 and 0.04 ± 0.01 in the inflamed and healthy muscles, respectively. The inflammation-to-muscle ratios of both tracers [^{18}F]FEAnGA-Me (1.48 ± 0.22) and [^{18}F]FEAnGA (1.59 ± 0.19) were not significantly different, but the tumor-to-muscle ratios of [^{18}F]FEAnGA-Me (1.85 ± 0.23) were significantly lower than those of [^{18}F]FEAnGA (3.53 ± 0.52, $P = .02$).

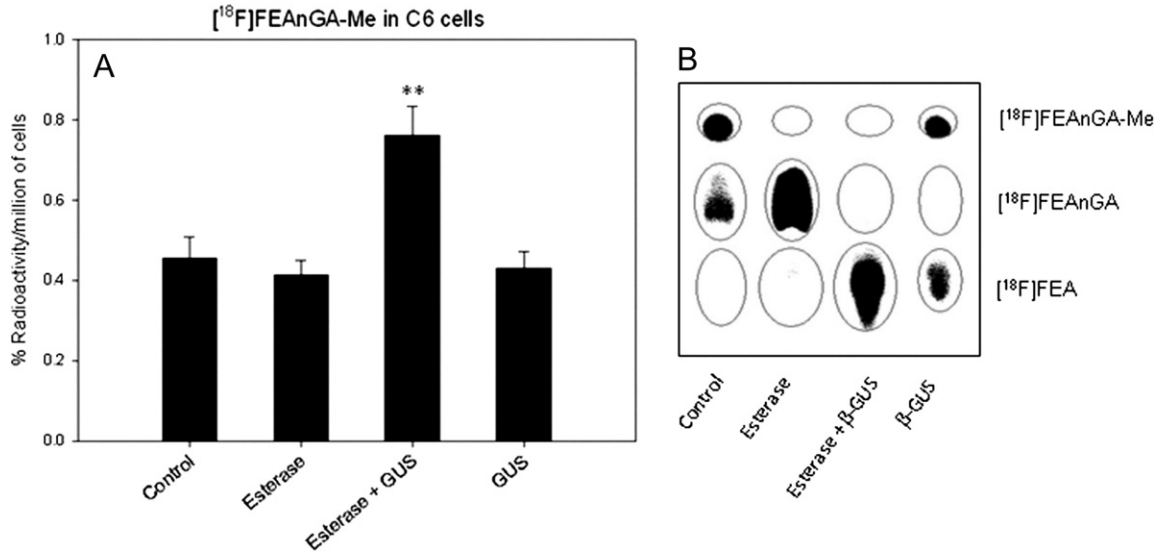

Fig. 3. A) Cell associated radioactivity of [^{18}F]FEAnGA-Me in control C6 cells and in C6 cells in the presence of *E. coli* β-GUS and/or esterase. Data are expressed as % uptake per million of cells presented in mean values of triplicate samples±SEM. $^{**}P < .005$, unpaired bidirectional Student's *t* test. B) Radio-TLC of medium samples of C6 cells.

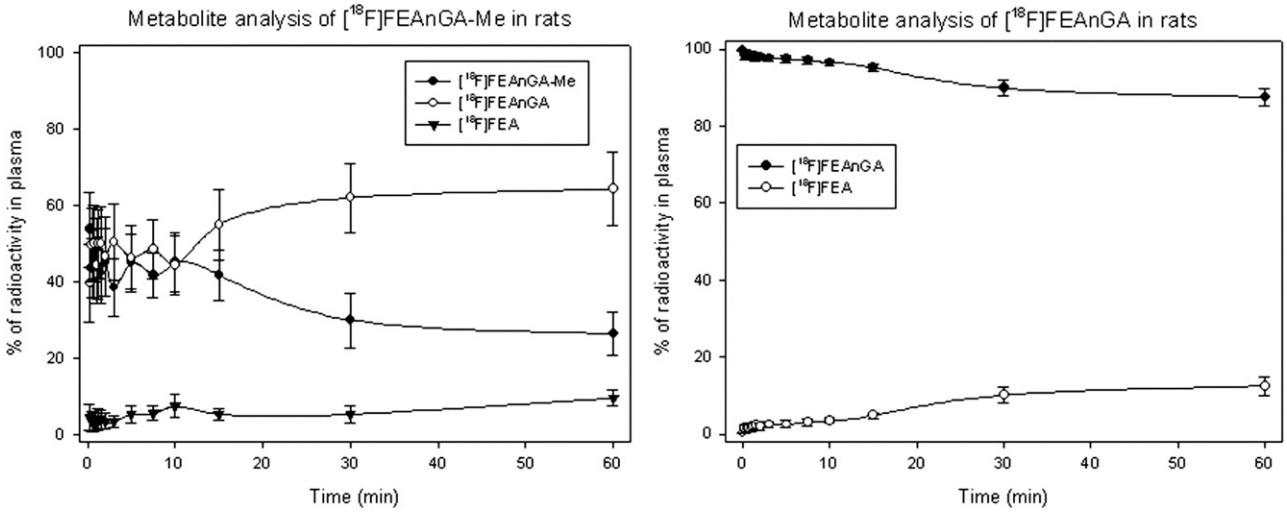

Fig. 4. Percentage of [^{18}F]FEAnGA-Me, [^{18}F]FEAnGA and [^{18}F]FEA in the plasma of rats at different time points after injection of [^{18}F]FEAnGA-Me (left, $n=8$) or [^{18}F]FEAnGA (right, $n=14$).

3.7. Pharmacokinetic modeling

The sampled rats were divided in two groups (injected with either [^{18}F]FEAnGA-Me or [^{18}F]FEAnGA) to compare the tracers' pharmacokinetics in vivo.

By applying 50% of SUV_{max} as the threshold, an ROI was obtained representing the viable part of the tumor. The TACs of the viable part of the tumor together with individual plasma radioactivity curves, Logan graphical analysis and a 2 tissue reversible compartment model were used for pharmacokinetic modeling.

The tumor distribution volume, DV_T, from the Logan graphical analysis after [^{18}F]FEAnGA-Me injection (0.61 ± 0.06), was not significantly different from the DV_T after [^{18}F]FEAnGA injection (0.50 ± 0.04). Similar distribution volumes were also obtained using the 2 tissue compartment modeling (Table 2).

3.8. Measurement of β-GUS activity

β-GUS activity was assessed by measurement of the release of HNBA from [^{18}F]FEAnGA-Me or [^{18}F]FEAnGA. β-GUS activity was analyzed in homogenates of excised whole tumors. The conversion of [^{18}F]FEAnGA to [^{18}F]FEA and HNBA in tumors was found to be similar whether injected with [^{18}F]FEAnGA-Me (0.35 ± 0.08 [HNBA]/mg of tissue) or [^{18}F]FEAnGA (0.35 ± 0.03 [HNBA]/mg of tissue).

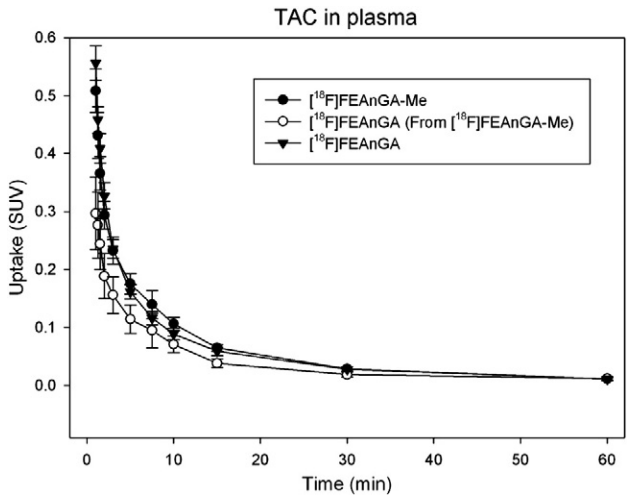

Fig. 5. The time activity curves of [^{18}F]FEAnGA-Me and [^{18}F]FEAnGA in plasma as a result of the i.v. administration of either [^{18}F]FEAnGA-Me or [^{18}F]FEAnGA.

4. Discussion

In the last years, interest into the development of radiolabeled markers for the non-invasive evaluation of prodrug-converting enzymes in solid tumors has increased [11–15]. Knowledge of the prodrug-converting enzyme expression and activity can lead to a better understanding of the mechanism of action and metabolic conversion of the prodrug and could identify sites that are prone to possible side-effects. Eventually, a suitable PET method might allow the selection of patients eligible for β-GUS mediated prodrug therapy. [^{18}F]FEAnGA is a PET tracer capable of detecting increased release of β-GUS in large solid tumors as well as in inflammatory lesions. However, the renal clearance of [^{18}F]FEAnGA was fast relative to the conversion of [^{18}F]FEAnGA to [^{18}F]FEA resulting in a relatively low tracer uptake in the tumor. Therefore, we synthesized the more lipophilic methyl ester of [^{18}F]FEAnGA, called [^{18}F]FEAnGA-Me and hypothesized that the increase in lipophilicity would prolong the circulation half-life of the tracer which would result in prolonged availability of the tracer for conversion by β-GUS.

The synthesis of [^{18}F]FEAnGA-Me was similar to [^{18}F]FEAnGA, only differing in the deprotection process where NaOMe/MeOH in anhydrous conditions was used instead of aqueous NaOH. This last step was of critical importance with regards to the final yield. In the presence of acetonitrile and NaOMe/MeOH the major compound obtained was [^{18}F]FEAnGA. However, if compound [^{18}F]-2 was dried before adding NaOMe/MeOH, [^{18}F]FEAnGA-Me was obtained in 5% to 10% yield. In addition, [^{18}F]FEAnGA was concomitantly formed in 5%–10% yield. Despite numerous attempts to improve the final yield, we were not able to improve the yield any further. Thus, the final product [^{18}F]FEAnGA-Me was obtained in 5%–10% overall radiochemical yield (corrected for decay, based on [^{18}F]fluoride) with a total synthesis time of 120 min (Scheme 2). The identity of [^{18}F]FEAnGA-Me was confirmed by coelution with a sample of the nonradioactive compound by RP-HPLC. [^{18}F]FEAnGA-Me was found to be completely stable in PBS for at least 1 h.

We anticipated that the methyl group of [^{18}F]FEAnGA-Me could be enzymatically converted to the carboxylic acid of [^{18}F]FEAnGA by esterase in the blood (Scheme 1). Indeed, we showed that [^{18}F]FEAnGA-Me was completely hydrolyzed to [^{18}F]FEAnGA in the

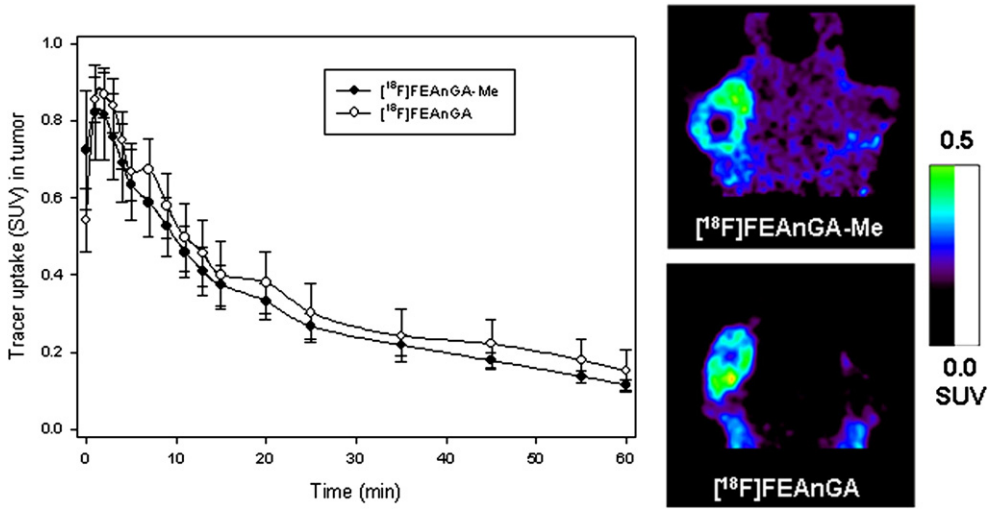

Fig. 6. Coronal microPET image of a rat injected with either [^{18}F]FEAnGA-Me or [^{18}F]FEAnGA on day 13 after inoculation of C6 cells (right side). Time activity curves of the tracer uptake (SUV) in the viable part of C6 gliomas after injection with either [^{18}F]FEAnGA-Me or [^{18}F]FEAnGA (left side).

presence of bovine liver esterase or rat plasma. Furthermore, intact [^{18}F]FEAnGA-Me itself was not a substrate of *E. coli* β-GUS. However, only after removal of the methyl group by esterase could complete conversion of the resulting [^{18}F]FEAnGA to [^{18}F]FEA be achieved by *E. coli* β-GUS. This result indicates that the activation of [^{18}F]FEAnGA-Me is a two-step process that requires both esterase and glucuronidase.

In vitro accumulation of [^{18}F]FEAnGA-Me was investigated in C6 glioma cells. The cell-associated radioactivity derived from [^{18}F]FEAnGA-Me was only increased in the presence of both esterase and *E. coli* β-GUS. There is no significant difference in the cell-associated radioactivity of cells incubated with [^{18}F]FEAnGA-Me alone or in the presence of either *E. coli* β-GUS or esterase. The radio-TLC analysis of the medium confirmed that this increase in cell uptake is associated with the conversion of [^{18}F]FEAnGA-Me to [^{18}F]FEA, since complete conversion of the tracer to [^{18}F]FEA was only observed when both esterase and β-GUS were present. C6 cells incubated with [^{18}F]FEAnGA-Me, in the presence of both esterase and *E. coli* β-GUS showed similar accumulation of radioactivity as C6 cells incubated with [^{18}F]FEA itself (0.8%) [2]. and 2 times higher uptake when compared to C6 cells incubated with [^{18}F]FEAnGA, in the presence of *E. coli* β-GUS (0.4%). However, the cellular uptake of [^{18}F]FEAnGA-Me in control C6 cells (absence of enzymes) was also higher than the uptake of [^{18}F]FEAnGA, suggesting a lower in vitro selectivity of [^{18}F]FEAnGA-Me when compared to [^{18}F]FEAnGA (Fig. 7).

As expected the lipophilicity of [^{18}F]FEAnGA-Me was found to be 10 fold higher than [^{18}F]FEAnGA. By analogy with the methyl ester DOX-mGA3 which was 3 times less hydrophilic than the original prodrug DOX-GA3, we hypothesized that the administration of the less hydrophilic [^{18}F]FEAnGA-Me would also result in a prolonged circulation of [^{18}F]FEAnGA in rats as compared to direct administration of the highly hydrophilic [^{18}F]FEAnGA.

Houba et al. found that the administration of methyl ester DOX-mGA3 in mice resulted in slow conversion of DOX-mGA3 to the original DOX-GA3 in plasma, resulting in slower plasma clearance and consequently, increased delivery and a higher concentration of DOX at the target site. In contrast to the encouraging results by Houba et al., we did not find any increase in radioactivity accumulation in the tumor after administration of the methyl ester PET tracer [^{18}F]FEAnGA-Me, when compared to the original tracer [^{18}F]FEAnGA. This apparent discrepancy could be explained by differences in the administered dose between the prodrug DOX-mGA (20,000 μg/kg) and the PET tracer [^{18}F]FEAnGA-Me (0.7 μg/kg). Conversion of glucuronide methyl esters by plasma esterases is generally a fast process. In the study by Houba et al., however, the administered dose was suggested to saturate the esterases in plasma, resulting in a relatively slow conversion of DOX-mGA3 to DOX-GA3. In contrast, the administrated amount of the glucuronide ester [^{18}F]FEAnGA-Me in our study was approximately 5 orders of magnitude lower and therefore far below the saturation level of plasma esterases. Indeed, [^{18}F]FEAnGA-Me was rapidly converted to [^{18}F]FEAnGA, as 50% conversion was already achieved within the first two minutes post injection. As a consequence, no difference in plasma AUC of [^{18}F]FEAnGA-Me and [^{18}F]FEAnGA was observed, nor were differences in the clearance half-life between both tracers observed.

Table 1
Ex vivo biodistribution 60 min p.i. of [^{18}F]-FEAnGA-Me or [^{18}F]FEAnGA in Wistar rats bearing a C6 tumor and a sterile inflammation.

	[^{18}F]FEAnGA-Me ($n=6$)	[^{18}F]FEAnGA ($n=8$)
Bone	0.05 ± 0.01	0.05 ± 0.02
Colon	0.26 ± 0.07	0.22 ± 0.07
Heart	0.16 ± 0.05	0.14 ± 0.06
Kidney	3.13 ± 0.67*	1.03 ± 0.48
Liver	0.97 ± 0.29*	0.34 ± 0.09
Lung	0.05 ± 0.01	0.12 ± 0.03
Pancreas	0.15 ± 0.08	0.11 ± 0.01
Spleen	0.17 ± 0.08	0.14 ± 0.03
Trachea	0.18 ± 0.07	0.13 ± 0.03
Plasma	0.13 ± 0.03	0.16 ± 0.06
Red blood cells	0.07 ± 0.02	0.06 ± 0.01
Muscle, control	0.08 ± 0.02	0.04 ± 0.01
Muscle, inflamed	0.13 ± 0.05	0.07 ± 0.02**
Tumor	0.13 ± 0.02**	0.13 ± 0.03***

Tracer uptake is expressed as standardized uptake values (SUV; mean ± SEM). *$P<.05$ [^{18}F]FEAnGA-Me when compared to [^{18}F]FEAnGA; **$P<.05$ and ***$P<.005$ when compared to control muscle.

Table 2
Pharmacokinetic parameters of both tracers and their conversion in C6 gliomas.

Parameters	[^{18}F]FEAnGA-Me ($n=7$)	[^{18}F]FEAnGA ($n=14$)
DV_{Logan} (mL/g)	0.61 ± 0.06	0.50 ± 0.04
DV_{2TCM} (mL/g)	0.63 ± 0.09	0.48 ± 0.04
[HNBA]/mg tissue	0.35 ± 0.08	0.35 ± 0.03

*$P<.05$ and **$P<.005$ when compared to administered [^{18}F]FEAnGA.

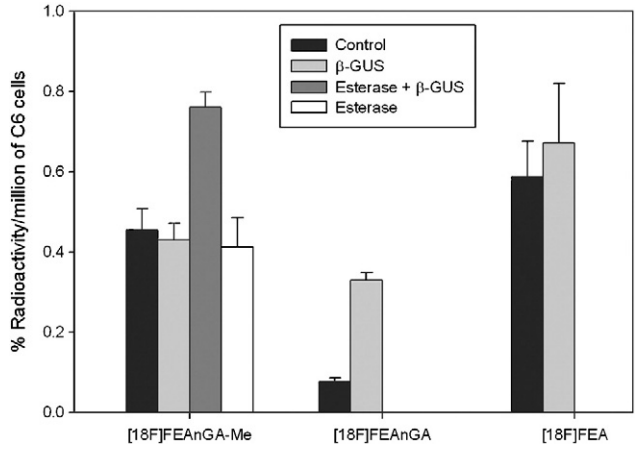

Fig. 7. Comparison of the uptake of [^{18}F]FEAnGA-Me, [^{18}F]FEAnGA and [^{18}F]FEA in C6 cells in the presence or absence of esterase and/or *E. coli* β-GUS.

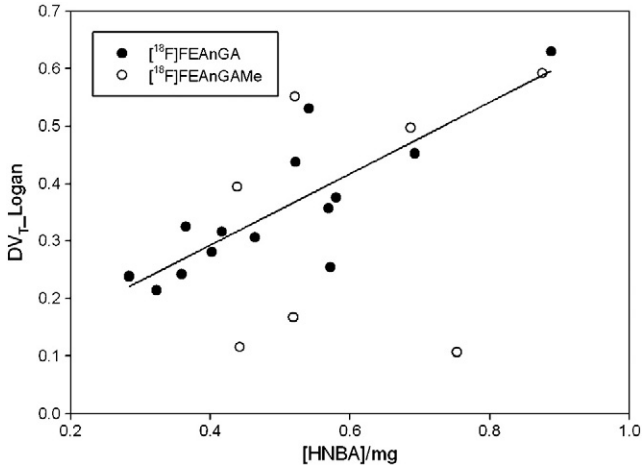

Fig. 8. Correlation between distribution volume in the viable part of the tumors calculated from a graphical model fit and rate of tracer cleavage determined in tissue homogenate, after the injection of either [^{18}F]FEAnGA ($y = 0.04 + 0.62x$, $R^2 = 0.69$, $P = .0002$) or [^{18}F]FEAnGA-Me ($y = 0.09 + 0.42x$, $R^2 = 0.11$, $P = .47$).

Metabolite analysis indicated initially rapid conversion of [^{18}F]FEAnGA-Me to [^{18}F]FEAnGA, but after 8 min the fraction of [^{18}F]FEAnGA in plasma stabilized. The late-phase slower conversion of [^{18}F]FEAnGA-Me in vivo might be attributed to initial rapid non-specific uptake of [^{18}F]FEAnGA-Me in tissue (as observed in vitro in the cellular uptake experiments in C6 cells), followed by slow redistribution of the methyl ester prodrug tracer into the circulation, where it is converted to [^{18}F]FEAnGA. This slow late phase conversion of the methyl ester prodrug is in agreement with observations by Houba et al. for DOX-mGA3.

The ex vivo biodistribution of both tracers indicated similar uptake (SUV) in most of the peripheral organs with the exception of the liver and kidneys, where the uptake was 3 times higher after injection of [^{18}F]FEAnGA-Me when compared with the uptake after injection with [^{18}F]FEAnGA. The uptake in inflamed muscle was 2 times higher after [^{18}F]FEAnGA-Me injection in comparison with the uptake after [^{18}F]FEAnGA injection. However, the uptake in healthy muscle was also 2 times higher in animals injected with [^{18}F]FEAnGA-Me. Thus, the ratio between inflamed and control muscle for the two tracers was similar. These biodistribution results are in agreement with what we found in vitro, where [^{18}F]FEAnGA-Me loses selectivity when compared to [^{18}F]FEAnGA suggesting an increased uptake of the less hydrophilic [^{18}F]FEAnGA-Me in normal tissue. Indeed, also in the pharmacokinetic analysis, no statistical differences were found between the distribution volumes (DV_T) in tumors when injected with one or either tracer.

When injected with [^{18}F]FEAnGA, DV_T in tumors is dependent on the [^{18}F]FEAnGA influx (from the plasma to the extracellular space) and its conversion to [^{18}F]FEA and HNBA in the presence of extracellular β-GUS. After [^{18}F]FEAnGA-Me injection the DV_T in tumors depends on both [^{18}F]FEAnGA-Me and [^{18}F]FEAnGA influx and the conversion of [^{18}F]FEAnGA to [^{18}F]FEA and HNBA. Therefore, as expected the DV_T in the viable part of the tumors correlated well with the HNBA formation after injection of [^{18}F]FEAnGA but did not correlate well with the HNBA formation when injected with [^{18}F]FEAnGA-Me (Fig. 8).

The pharmacokinetic behavior of [^{18}F]FEAnGA-Me is likely more favorable in man considering the lower levels of esterase in the human body as compared to rats which would increase the availability of the tracer for β-GUS. However, these sustained plasma levels of tracer would ultimately increase the background activity and therefore decrease the contrast between background and targeted region. Therefore, different strategies should be pursued in order to improve the pharmacokinetics of glucuronide PET tracers, such as PET tracers with higher turn over so that the release of the radioactive moiety is faster than the clearance of the tracer, resulting in higher tracer uptake at the target site without increasing the background activity.

5. Conclusion

[^{18}F]FEAnGA-Me was labeled with [^{18}F]fluoride and has a high in vitro stability in PBS. [^{18}F]FEAnGA-Me proved to be a good substrate for plasma esterase and in the presence of both esterase and *E. coli* β-GUS is converted to [^{18}F]FEA and HNBA. In contrast to our hypothesis, administration of [^{18}F]FEAnGA-Me did not result in a significantly prolonged circulation of [^{18}F]FEAnGA in rats as compared to the direct administration of [^{18}F]FEAnGA. In fact, due to its lower hydrophilicity, nonspecific uptake of [^{18}F]FEAnGA-Me increased, resulting in a lower target to background contrast. In addition, the 2-step prodrug activation strategy further complicates the mode of action of this radiopharmaceutical and thus complicates the interpretation of the imaging results. Therefore, different strategies, such as the use of prodrug with higher β-GUS turnover should likely be pursuit in order to improve the pharmacokinetics and pharmacodynamics of glucuronide PET tracers.

Acknowledgments

We gratefully thank Katica Stojanov and Zhila Mosheini for their help in the C6 glioma cell studies.

References

[1] Antunes IF, Haisma HJ, Elsinga PH, Dierckx RA, de Vries EFJ. Synthesis and evaluation of [18F]-FEAnGA as a PET Tracer for beta-glucuronidase activity. Bioconjugate Chem 2010;21:911–20.
[2] Antunes IF, Haisma HJ, Elsinga PH, van Waarde A, Willemsen ATM, Dierckx RA, de Vries EFJ. In vivo evaluation of 1-*O*-(4-(2-fluoroethyl-carbamoyloxymethyl)-2-nitrophenyl)-*O*-b-D-glucopyronuronate: a positron emission tomographic tracer for imaging b-glucuronidase activity in a tumor/inflammation rodent model. Molecular Imaging 2011 [in press].
[3] Houba PH, Boven E, van der Meulen-Muileman IH, Leenders RG, Scheeren JW, Pinedo HM. Distribution and pharmacokinetics of the prodrug daunorubicin-GA3 in nude mice bearing human ovarian cancer xenografts. Biochem Pharmacol 1999;57:673–80.
[4] Houba PH, Boven E, van der Meulen-Muileman IH, Leenders RG, Scheeren JW, Pinedo HM. A novel doxorubicin-glucuronide prodrug DOX-GA3 for tumour-selective chemotherapy: distribution and efficacy in experimental human ovarian cancer. Br J Cancer 2001;84:550–7.
[5] de Graaf M, Nevalainen TJ, Scheeren HW, Pinedo HM, Haisma HJ, Boven E. A methylester of the glucuronide prodrug DOX-GA3 for improvement of tumor-selective chemotherapy. Biochem Pharmacol 2004;68:2273–81.

[6] Tewson TJ. Synthesis of [18F]fluoroetanidazole: a potential new tracer for imaging hypoxia. Nucl Med Biol 1997;24:755–60.
[7] van Waarde A, Cobben DC, Suurmeijer AJ, Maas B, Vaalburg W, de Vries EFJ. Selectivity of 18F-FLT and 18F-FDG for differentiating tumor from inflammation in a rodent model. J Nucl Med 2004;45:695–700.
[8] Van Waarde A, Jager PL, Ishiwata K, Dierckx RA, Elsinga PH. Comparison of sigma-ligands and metabolic PET tracers for differentiating tumor from inflammation. J Nucl Med 2006;47:150–4.
[9] Krak NC, Boellaard R,, Hoekstra OS, Twisk JW, Hoekstra CJ, Lammertsma AA. Effects of ROI definition and reconstruction method on quantitative outcome and applicability in a response monitoring trial. Eur J Nucl Med Mol Imaging 2005;32:294–301.
[10] Soret M, Bacharach SL, Buvat I. Partial-volume effect in PET tumor imaging. J Nucl Med 2007;48:932–45.
[11] Buursma AR, van Dillen IJ, van Waarde A, Vaalburg W, Hospers GA, Mulder NH. Monitoring HSVtk suicide gene therapy: the role of [(18)F]FHPG membrane transport. Br J Cancer 2004;91:2079–85.
[12] Celen S, Deroose C, de Groot T, Chitneni SK, Gijsbers R, Debyser Z. Synthesis and evaluation of 18F- and 11C-labeled phenyl-galactopyranosides as potential probes for in vivo visualization of LacZ gene expression using positron emission tomography. Bioconjug Chem 2008;19:441–9.
[13] de Vries EFJ, Buursma AR, Hospers GA, Mulder NH, Vaalburg W. Scintigraphic imaging of HSVtk gene therapy. Curr Pharm Des 2002;8:1435–50.
[14] Fei X, Wang JQ, Miller KD, Sledge GW, Hutchins GD, Zheng QH. Synthesis of [18F] Xeloda as a novel potential PET radiotracer for imaging enzymes in cancers. Nucl Med Biol 2004;31:1033–41.
[15] Furumoto S, Takashima K, Kubota K, Ido T, Iwata R, Fukuda H. Tumor detection using 18F-labeled matrix metalloproteinase-2 inhibitor. Nucleic Med Biol 2003;30:119–25.